Examination of the skin barrier repair/wound healing process using a living skin equivalent model and matrix-assisted laser desorption-ionization-mass spectrometry imaging

E. E. L. Lewis*,†, M. R. T. Barrett*, L. Freeman-Parry†, R. A. Bojar* and M. R. Clench† [ID]

*Innovenn UK Ltd., National Agri-Food Innovation Campus, Sand Hutton, York YO41 1LZ, U.K. and †Centre for Mass Spectrometry Imaging, Biomolecular Sciences Research Centre, Sheffield Hallam University, 754 Owen Building, City Campus, Howard Street, Sheffield S1 1WB, U.K.

Abstract

OBJECTIVE: Examination of the skin barrier repair/wound healing process using a living skin equivalent (LSE) model and matrix-assisted laser desorption/ionization-mass spectrometry imaging (MALDI-MSI) to identify lipids directly involved as potential biomarkers. These biomarkers may be used to determine whether an *in vivo* wound is going to heal for example if infected.
METHODS: An *in vitro* LSE model was wounded with a scalpel blade and assessed at day 4 post-wounding by histology and MALDI-MSI. Samples were sectioned at wound site and were either formalin-fixed paraffin-embedded (FFPE) for histology or snapped frozen (FF) for MSI analysis.
RESULTS: The combination of using an *in vitro* wounded skin model with MSI allowed the identification of lipids involved in the skin barrier repair/wound healing process. The technique was able to highlight lipids directly in the wound site and distinguish differences in lipid distribution between the epidermis and wound site.
CONCLUSION: This novel method of coupling an *in vitro* LSE with MSI allowed in-depth molecular analysis of the skin barrier repair/wound healing process. The technique allowed the identification of lipids directly involved in the skin barrier repair/wound healing process, indicating these biomarkers may be potentially be used within the clinic. These biomarkers will help to determine, which stage of the skin barrier repair/wound healing process the wound is in to provide the best treatment.

Résumé

OBJECTIF: Examen de la réparation de la barrière cutanée/processus de cicatrisation en utilisant un modèle d'équivalent de peau vivante (LSE) et l'imagerie par spectrométrie de masse assistée par désorption-ionisation laser (MALDI-MSI) pour identifier les lipides directement impliqués comme biomarqueurs potentiels. Ces biomarqueurs peuvent être utilisés par exemple pour déterminer si une plaie in vivo va guérir si elle est infectée.
MÉTHODES: Un modèle de LSE in vitro a été blessé avec une lame de scalpel et analysé au jour 4 après la blessure par histologie et MALDI-MSI. Ces échantillons de tissu étaient soit fixés au formol et inclus dans la paraffine (FFPE) pour l'histologie, soit congelés (FF) pour l'analyse MSI.
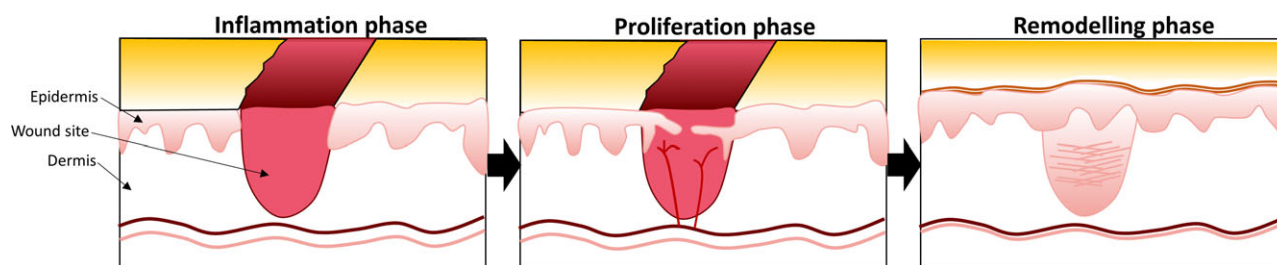**RÉSULTATS:** L'utilisation d'un modèle de peau blessée in vitro couplé avec la MSI a permis l'identification des lipides impliqués dans le processus de réparation de la barrière cutanée/cicatrisation. La technique a permis de mettre en évidence les lipides directement au niveau de la plaie et de distinguer les différences de distribution des lipides entre l'épiderme et le site de la plaie.
CONCLUSION: Cette nouvelle méthode de couplage d'un modèle LSE in vitro avec la MSI a permis une analyse moléculaire approfondie de la réparation de la barrière cutanée/processus de cicatrisation. La technique a permis l'identification de lipides directement impliqués dans la réparation de la barrière cutanée/processus de cicatrisation, indiquant que ces biomarqueurs peuvent être potentiellement utilisés en clinique. Ces biomarqueurs aideront à déterminer à quel stade de la réparation de la barrière cutanée/processus de cicatrisation de la plaie se trouve le meilleur traitement.

Correspondence: M. R. Clench, Centre for Mass Spectrometry Imaging, Biomolecular Sciences Research Centre, Sheffield Hallam University, 754 Owen Building, City Campus, Howard Street, Sheffield S1 1WB, U.K. Tel.: +44 (0)114 225 3054; fax: +44 (0)114 225 3066; e-mail: m.r.clench@shu.ac.uk

Introduction

Damage to the structural integrity of the skin through trauma or injury initiates the skin barrier repair/wound healing process, which is highly complex and carefully regulated with ordered responses [1]. There are four main stages involved in the normal skin barrier repair/wound healing process: haemostasis, inflammation, proliferation and remodelling, all of which occur in an overlapping chronological sequence as shown in Fig. 1 [2]. Disruption to the sequence or prolongation in the inflammation stage has been shown to delay the skin barrier repair/wound healing process, leading to non-healing chronic wound formation. Chronic wounds have been described as wounds, which do not heal within 3 months from the time of injury [3]. Several factors have been shown to affect the progression of the normal skin barrier repair/wound healing process, including infection, age, diabetes and obesity [4]. The prevalence of chronic wounds has been described as a silent epidemic, affecting a large proportion of the world population, particularly western societies, where 1–2% of the population will develop a chronic wound [5]. Treating and managing these wounds creates major problems for health budgets in the western

Figure 1 Schematic diagram of the normal skin barrier repair/wound healing process from the inflammation stage leading to the proliferative stage and then the remodelling stage.

world, where a total cost of 2–4% is spent caring for people suffering from these wounds [5]. These health problems cause a huge drain on wound care management resources and in 2014 the UK's National Health Service spent approximately £2.17 billion on wound care services [6]. Unfortunately, the health budgets in western countries are expected to rise annually, as a natural consequence of ageing populations and an increase in people suffering from diabetes and obesity. Severe pain, sepsis, hospitalization and in some cases amputations are factors affecting patients with chronic wounds [7]. Research has suggested that better diagnosis and wound management may prevent chronic wound formation [8]. This paper reports the creation of *in vitro* 3D wounded skin models using living skin equivalent (LSE) models. These are easily manipulated to create wounds in a controlled environment. The use of matrix-assisted laser desorption ionization-mass spectrometry imaging (MALDI-MSI) to study these wound models provides the opportunity for unlabelled multi-analyte detection capable of analysing a wide range of molecules simultaneously, whilst assessing the spatial distribution of molecules in biological tissues [9]. In this paper, a wounded LSE model was combined with MALDI-MSI to discover and identify biomarkers specific to the skin barrier repair/wound healing process. These biomarkers have the potential to be applied within clinics as an early diagnostic tool to help identify whether a wound is healing or developing into a chronic wound.

Materials and methods

Incision wound protocol

The incision model was created using a commercial LSE model (Labskin; Innovenn UK Ltd., York, U.K.) at day 12 air-liquid interface. Each sample was wounded three times with a scalpel blade (No 10; Swann-Morton, Sheffield, U.K.) at controlled penetration wounding the epidermal and dermal layers. Samples were assessed at day 4 post-wounding.

Media was changed every 2 days with Labskin maintenance medium (Innovenn UK Ltd.) up to 4 days post-wounding.

Fresh frozen tissue and cryosectioning

At day 4, samples were removed from the well plate inserts, detached from the membrane and cut in half across the wound site and embedded in 20% gelatine (Sigma Aldrich, Poole, U.K.) within a silicone mould (Truffly Made Inc., Coronado, U.S.A.). The silicone mould was placed directly on a polystyrene float in a

polystyrene box containing liquid nitrogen. The samples were removed from the mould once snap frozen and stored at −80°C for at least 24 h prior to sectioning. Each sample was divided into two and each half was mounted onto cork rings with deionized water at −25°C. Samples were cryosectioned at 10 μm directly across the wound site and freeze-thaw mounted onto either polylysine-coated microscope slides (SLS, Nottingham, U.K.) for analysis on either the Waters Synapt G2 HDMS or the Applied Biosystems QSTAR Pulsar *i* mass spectrometers or indium titanium oxide (ITO) coated slides for analysis on the Bruker Autoflex III mass spectrometer.

Formalin-fixed paraffin-embedded (FFPE) tissue and sectioning

Samples were fixed with 10% neutral buffered formalin (Genta Medical, York, U.K.) and processed using a dehydration series in different concentrations of industrial denatured alcohol (IDA; Genta Medical) each for 1 h (70%, 80% and 90%) and then 100% IDA for 1 h (×3), xylene substitute for 1 h (×3) and then paraffin wax at 58°C for 1 h (×2). Samples were embedded in paraffin wax and sectioned at 5 μm using a microtome HM 325 (Thermo Fisher, Warrington, U.K.) onto microscope slides. Samples were left in a 50°C oven overnight prior to staining.

Haematoxylin and eosin staining

Formalin-fixed paraffin-embedded samples slides were placed in xylene substitute for 5 min twice, 100% IDA for 3 min twice and rinsed with tap water for 5 min. Slides were transferred to Harris haematoxylin (Cell Path, Newton, U.K.) for 10 min, rinsed with tap water for 2 min and then dipped into 1 : 1 v/v 0.5% acid alcohol: 70% IDA for 3 s. Slides were then rinsed for 3 min with tap water, placed in Scott's tap water for 1 min and then rinsed with tap water for 3 min. The slides were transferred to eosin y solution for 3 min and then rinsed with tap water for 2 min. Slides were dipped into 70% IDA for 3 s, transferred to 100% IDA for 3 min twice and then xylene substitute for 3 min twice. Samples were mounted with DPX and imaged using a Leica DM2000 microscope fitted with 4×, 10×, 20×, 40× and 100× objectives and analysed with Leica LAS X software (Nussloch, Germany).

Fresh frozen tissue samples were washed with 100% acetone for 5 min twice and then rinsed with tap water for 5 min. The same protocol was followed as described above after transferring the samples to Mayers haematoxylin (VWR) for 10 min to mounting the samples with DPX.

Small-molecule MALDI-MS imaging

Positive ion mode

Sections were coated with MALDI matrix (α-cyano-4-hydroxycinnamic acid (CHCA; Sigma Aldrich), 5 mg mL^{-1} in 70 : 30 acetonitrile: 0.5% TFA) using a SunCollect (SunChrom, Friedrichsdor, Germany) sprayer. Slides were coated with eight layers of CHCA matrix, spraying at 4 μL min^{-1} for the first layer and then 3.5 μL min^{-1} for the subsequent seven layers. Mass spectra was collected on an Applied Biosystems/MDS Sciex hybrid quadrupole TOF mass spectrometer (QSTAR Pulsar *i*) with an orthogonal MALDI ion source (Applied Biosystems, Foster City, CA, U.S.A.) and a high-repetition neodymium-doped yttrium aluminium garnet (Nd : YAG) laser (355 nm, 1 KHz) (Applied Biosystems). Image acquisition was performed at a pixel size of 75 $\times$ 75 μm in 'Raster Image' mode with mass range of 400–1200 Da. Images were generated using the freely available Novartis BIOMAP 3.8.0.4 software (www.maldi-msi.org). Prior to analysis, the instrument was calibrated using αCHCA matrix peak cluster ions.

Negative ion mode for Imaging

Sections were coated with MALDI matrix [N-(1-naphthyl) ethylenediamine dihydrochloride monomethanolate (NEDC; Sigma Aldrich), 7 mg mL^{-1} in 1 : 1 methanol : deionized water] using a SunCollect (SunChrom) sprayer. Slides were coated with six layers of NEDC matrix, spraying each layer at 3.5 μL min^{-1}. Mass spectra were collected on a Bruker Autoflex III fitted with a 'Smartbeam' Nd : YAG laser (355 nm, 1 KHz) (Bruker, Bremen, Germany). Image acquisition was performed at a pixel size of 30 $\times$ 30 μm in 'Raster Image' mode with a mass range of 400–1200 Da. Prior to analysis, the instrument was calibrated using the Bruker prepared mtp standard target peptide calibration mix 2.

Negative ion mode for MS/MS profiling

Sections were coated NEDC as described above, however, samples were analysed using a HDMS SYNAPT G2 HDMS system (Waters Corporation, Manchester, U.K.) and DRIFTSCOPE 2.1 software (Waters
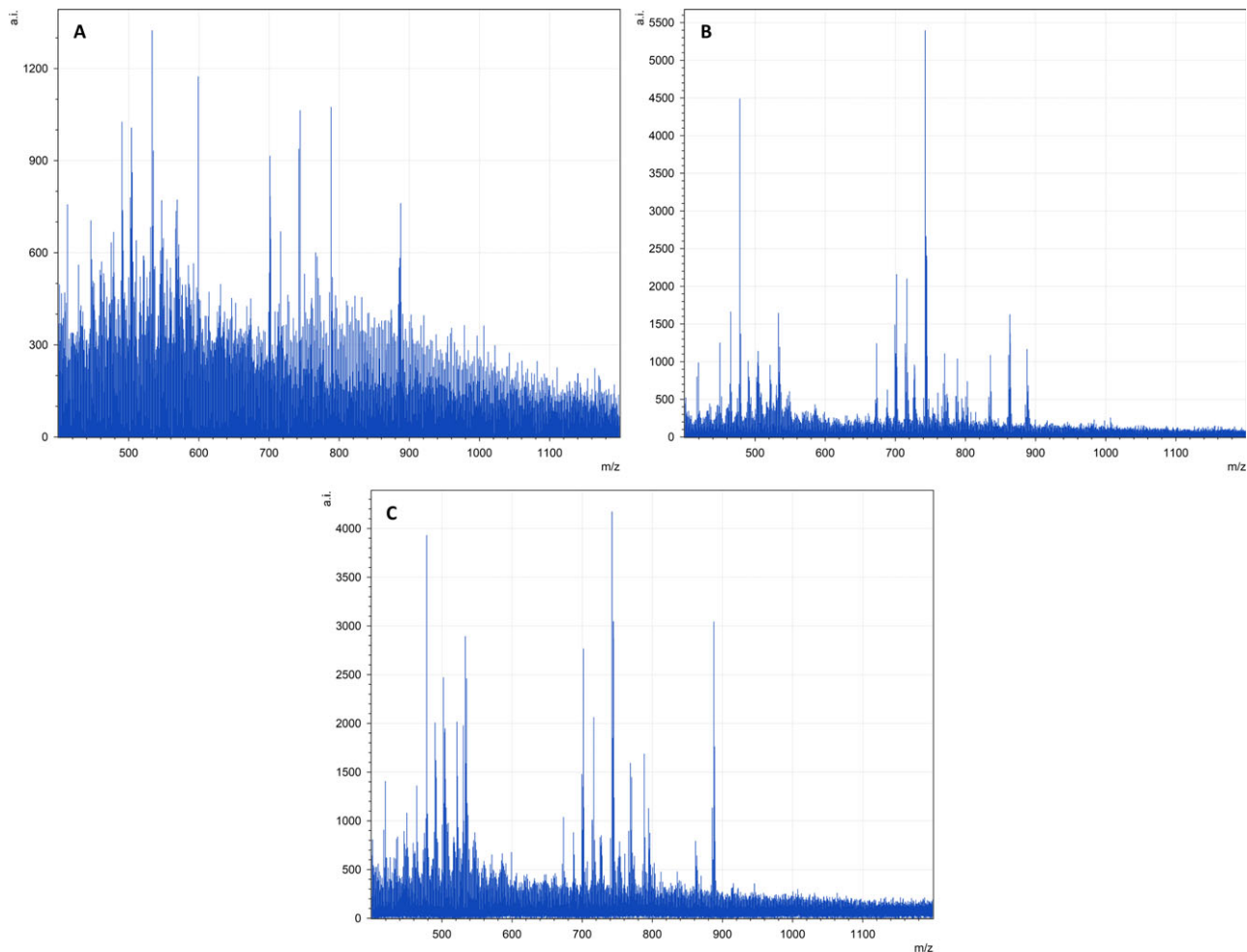
Figure 2 Matrix-assisted laser desorption-ionization-mass spectrometry profiling within the *m/z* 400–1200 range for all three regions of interest in negative ion mode. (A) Dermis, (B) epidermis and (C) wound Site.
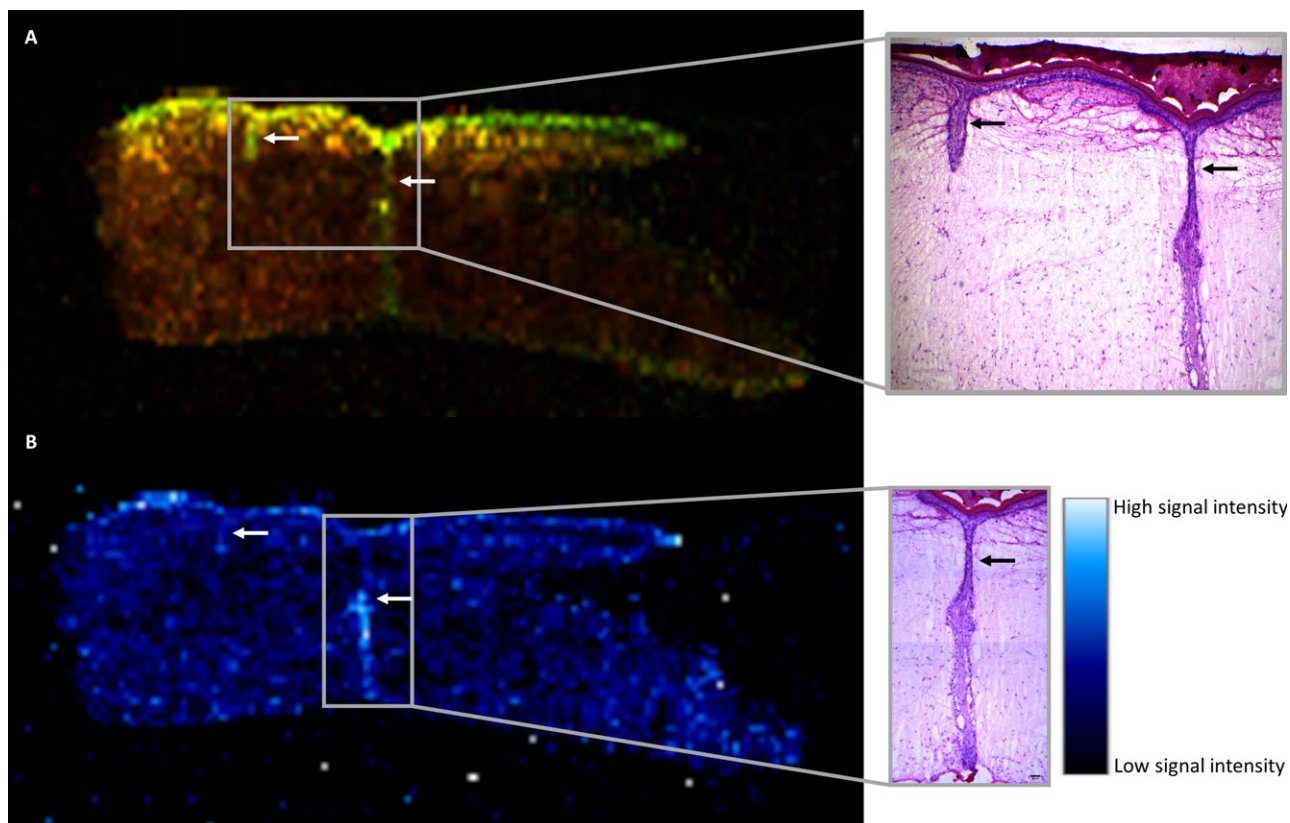
Figure 3 Mass spectrometry imaging of incision model 4 days post wounding showing the spatiotemporal distribution of three species across the tissue in positive ion mode. White and black arrows show the two wound sites in the image (A) Bi-colour image of two distinct ion species in the epidermis (green = m/z 721.4) and dermis (red = m/z 725.4). H&E image of same sample, 4× magnification. (B) MSI of spatiotemporal distribution of an ion species with m/z 751.6 value across the tissue, the colour intensity relates to signal intensity in a pixel location.

Corporation). MS/MS spectra were acquired by manually moving the laser position and adjusting the collision energy between 25–45 eV with acquisition times of 20 s per spectrum. MS/MS peak lists from each spectrum were uploaded onto LIPID MAPS (http://www.lipidmaps.org) for database search. Prior to analysis, the instrument was calibrated using red phosphorous cluster ions.

Results

Mass spectrometry profiling and imaging of localized lipids

The technique was used to assess the lipid distribution across the wounded sample with emphasis on three regions of interest (ROIs); (i) the dermis, (ii) the wound site and (iii) the epidermis. The main area of interest was the wound site, which was compared to the dermis and the epidermis to determine lipid profile differences in the three ROIs. Figure 2 shows the average mass spectra collated from each ROI showing m/z peaks of signals, which are potentially lipids in the m/z range 400–1200. This allowed for the creation of MS profile signatures, which were distinct between the dermis, wound site and epidermis. The spectra from the dermis layer exhibited a limited number of m/z peaks compared to the wound site and the epidermis. The results show similarities in the m/z values

identified in the wound site and epidermal spectra. However, the wound site mass spectra exhibited a greater number of peaks in the lower mass range compared to those acquired from the epidermis.

The haematoxylin and eosin (H&E) staining of the tissue showed that keratinocytes from the epidermis had migrated into the wound site, providing an explanation for the similarities in mass spectra acquired from the epidermis and the wound site (Fig. 3).

MS images of the distribution of (A) m/z 721.4 and 725.4 (as a bicolour overlay) and (B) m/z 751.6 are shown in Fig. 3 from the tissue sample 4 days post-wounding. In the images, the epidermis is clearly visible as a layer in the upper part of each image. Two of three wound sites present in the sample can also be seen in the images and have been highlighted in Fig. 3 with black and white arrows. In Fig. 3(A) the ion distribution shown in the image in green represents a species with a m/z value of 721.4 and can be observed to localize in keratinocytes in the epidermis as well as in the wound site. Additionally, the ion shown in Fig. 3(A) in red (m/z 725.4) was only found in the dermis. Figure 3(B) shows the spatial distribution of a single ion (m/z 751.6) and shows that the signal is predominately located within the healed wound site, by comparison with the H&E image of the same tissue (Fig. 3B inserts).
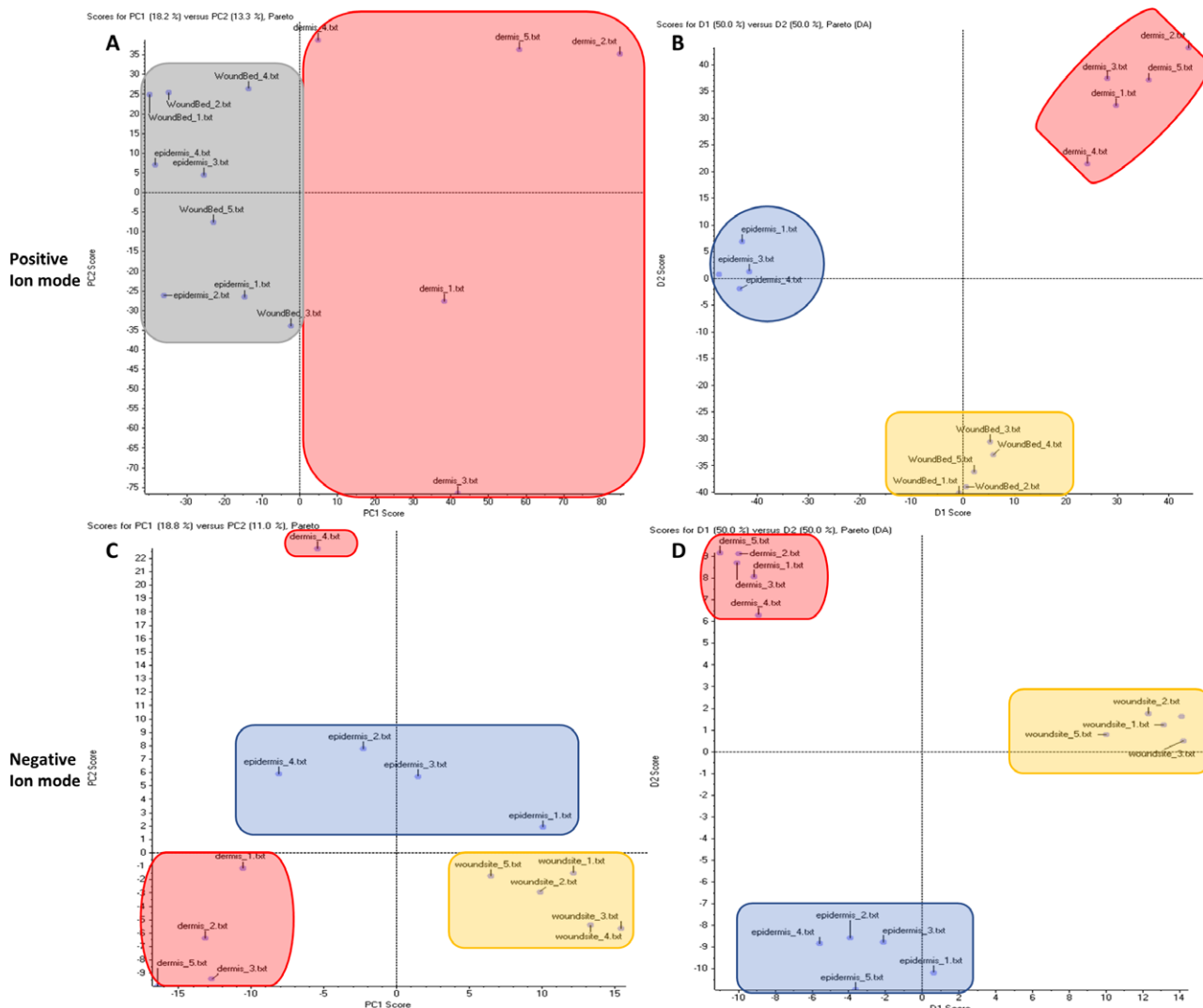
Figure 4 PCA and PCA-DA score plots obtained from data collected from all three regions of interest (dermis, wound site and epidermis) in positive and negative ion mode. (A) PCA scores plot in positive ion mode, (B) PCA-DA scores plot in positive ion, (C) PCA scores plot in negative ion mode and (D) PCA-DA scores plot in negative ion mode. Dermis (red), yellow (wound site), blue (epidermis) and green (wound site and epidermis). PCA, principal component analysis; DA, discriminant analysis.

Principal component analysis-discriminant analysis

To investigate whether there were distinct lipids from each region of interest, all the spectra collated from the tissue were subjected to principal component analysis (PCA) and principal component analysis-discriminant analysis (PCA-DA). A spectrum was collected at every single point as the laser was fired across the sample. Therefore, the spectrum contained all the information relating to all signal intensities of the ions within the selected mass range. A vast amount of information was collected from the whole tissue, creating a large dataset for each analysed sample. PCA reduced the dimensionality of the dataset allowing the data to be interpreted, whilst retaining all the statistical information. PCA-DA is a supervised variant of PCA and allowed groups to be

discriminated using multiple observed variables (e.g. discriminating between dermis, wound site and epidermis) if unsupervised PCA was unable to distinguish statistical differences between the three ROI. Figure 4 shows PCA and PCA-DA plots of 5 spectra datasets from each ROI (dermis, wound site and epidermis) in positive and negative ion mode. The spectra from each ROI were chosen by assessing the H&E image to select regions, which were distinct from each other. Figure 4(A–D) shows the PCA and PCA-DA scores plots obtained from these data. Figure 4(A) shows PCA scores plot for positive ion mode and showed there were differences in ions from the dermis (region highlighted in red), compared to the wound site and epidermis. However, there was very little variation between the wound site and the epidermis (region highlighted in green). However, the PCA-DA scores plot (Fig. 4B)
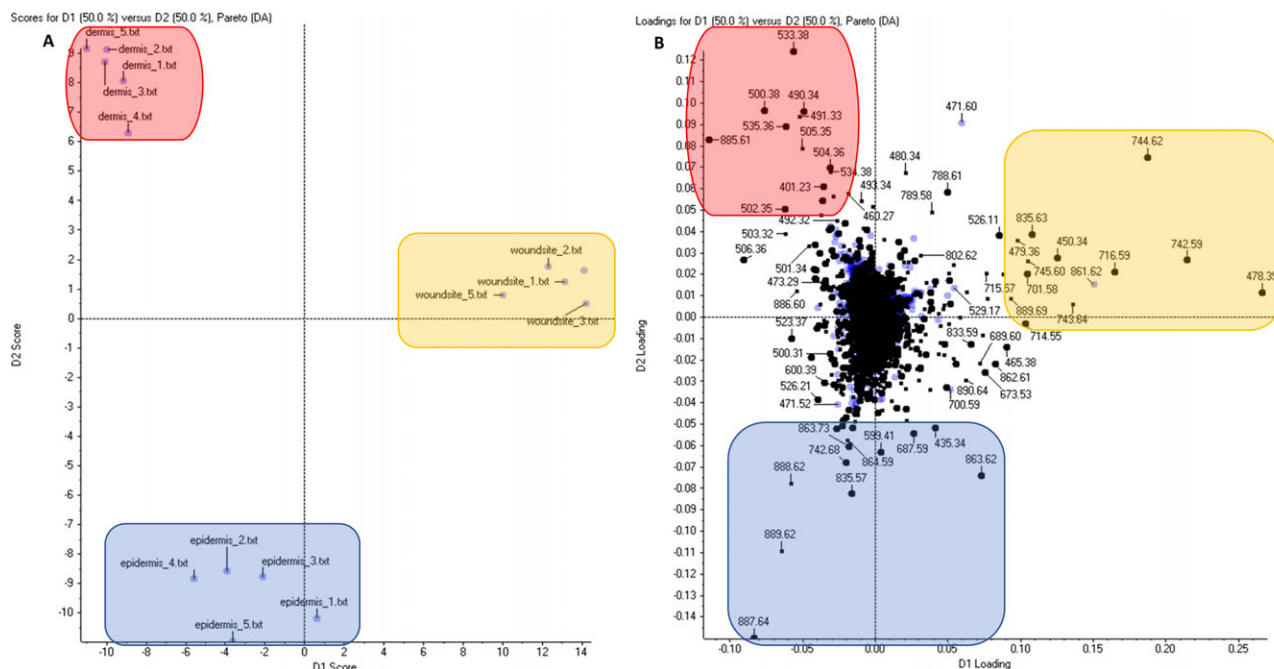
Figure 5 (A) PCA-DA scores plot and (B) PCA-DA loadings plot from the negative ion data representing all three regions of interest [dermis (red), yellow (wound site) and blue (epidermis)]. PCA; principal component analysis; DA, discriminant analysis.

showed discrimination between the three ROIs, indicating there were distinct ions and potentially lipids associated with each area (red area for dermis, yellow area for wound site and blue area for epidermis). Figure 4(C) shows the PCA scores plot conducted on spectra collected from the selected ROIs in negative ion mode and showed there were specific ions related to each ROI because it was able to separate the regions without group information. However, the spectrum from one dermis ROI was very dissimilar from the other dermis spectra. PCA-DA, shown in Fig. 4(D) was able to discriminate between all three ROI based on the ions within each ROI.

Figure 5 shows the PCA-DA scores and loadings plots from the negative ion data. Using the loadings plot, individual ions associated specifically with each region were identified. The PCA-DA allowed the individual ions isolated in each ROI to be compared against a lipid database based on its m/z value. Therefore, allowing putative identification of specific lipids in each region as shown in Table I.

Several isobaric lipids were identified from each m/z value due to molecules possessing the same molecular mass, but different structures. Therefore, it was difficult to identify the exact lipid based on its m/z value alone without further investigation such as conducting tandem mass spectrometry (MS/MS) profiling.

MS/MS profiling of putative lipids

Eleven m/z values were selected from Table I where four represented the dermis, four from the epidermis and three from the wound site for MS/MS analysis. It was possible to identify five species based on their product ion spectra as shown in Table II. Four of the putative identified lipids belonged to the group of lipids called

glycerophospholipids [e.g. phosphatidylethanolamines (PE), phosphatidylserines (PS), phosphatidylgylcerols (PG), phosphatidic acids (PA) and phosphatidylinositols (PI)] and were located in the dermis and wound site. Whereas, a glucosylceramide (Glcβ-Cer) was found in the epidermis and wound site and belonged to a group of lipids called glycosphingolipids.

Metabolite Pathway database searching

Mass-to-charge ratios and averaged signal intensities from spectra of each ROI were submitted to Pathos, which is a database to identify metabolites in numerous metabolic pathways based on their m/z values. It was possible to compare spectra from the wound site against the dermis to highlight potential metabolites, which may be involved in the skin barrier repair/wound healing process as shown in Table III. The Pathos search found 14 metabolites involved in nine different pathways with 42% of them involved in the biosynthesis of unsaturated fatty acids and ubiquinone biosynthesis, as well as purine metabolism. All the metabolites identified in the pathways showed an increased change in signal intensity, indicating there was an increase in metabolite production and/or secretion in the wound site.

Discussion

Recently, there has been a vast amount of interest in the study of lipids, which has led to the development of a newly emerging field of research called lipidomics [10]. This area of studying lipids includes the large-scale quantitative and qualitative analysis of different lipid classes and individual lipid species [11]. Lipids are part of the metabolome and are fundamental and important in many

Table I List of putative identification of ions from PCA-DA in negative ion mode in all three ROIs (dermis, wound site and epidermis) using LIPID MAPS structure database search (mass tolerance ±0.02 Da)

Location	m/z	Theoretical m/z	m/z error	Putative identification
Dermis	491.33	491.3143	0.0157	PA
		491.3531	0.0231	Xeniasterol-a
		491.3742	0.0442	1alpha, 25-dihydroxy-11alpha-phenylvitamin D3
	504.36	504.3460	0.014	PC
		504.3460	0.014	CerP
	504.39	504.3460	0.014	CerP
		504.3460	0.014	PC
	505.35	505.3171	0.0329	2-deoxy-20-hydroxy-5alpha-ecdysone 3-acetate
		505.3899	0.0399	(20R/S)-24-Hydroxy-19-norgeminivitamin D3
	533.38	533.4212	0.0412	DG
		533.4153	0.0353	Torulene
		533.3848	0.0048	Cholesteryl-alpha-D-glucoside
		533.4153	0.0353	3,4-Didehydro-beta-carotene
		533.4153	0.0353	3,4-Dehydrolycopene
		533.4153	0.0353	1′,2′-Dihydrochlorobactene
	534.38	534.3565	0.0235	PC
		534.3565	0.0235	PE
		534.3565	0.0235	LysoPE
		534.3953	0.0153	11alpha-(4-dimethylaminophenyl)-1alpha,25-dihydroxyvitamin D3
	885.61	885.6260	0.016	PGS
		885.6590	0.049	PG
	885.71	885.6978	0.0122	TG
Wound site	478.39	478.3902	0.0002	Docosadienoylcarnitine
		478.4266	0.0366	Cer
	716.59	716.5600	0.03	PC
		716.5600	0.03	PE
	717.67	717.6403	0.0297	DG
		717.6555	0.0145	22 : 2 Campesteryl ester
	742.59	742.5756	0.0144	PC
		742.5756	0.0144	PE
		742.5756	0.0144	PnC
		742.5475	0.0425	Termitomycesphin A
		742.5839	0.0061	GlcCer
	744.62	744.5913	0.0287	PC
		744.5913	0.0287	PE
	887.79	887.8073	0.0173	TG
Epidermis	699.65	699.6086	0.0414	22 : 4 Cholesteryl ester
		699.6086	0.0414	20 : 3 Stigmasteryl ester
	835.57	835.5495	0.0205	PG
		835.534	0.036	PI
	861.79	861.7917	0.0017	TG
	863.71	863.7134	0.0034	TG
		863.6770	0.033	22 : 3-Glc-cholesterol
		863.6770	0.033	20 : 2-Glc-Stigmasterol
		863.6770	0.033	20 : 3-Glc-Sitosterol
	887.64	887.6747	0.0347	PG
	888.62	888.6488	0.0288	PC
		888.6699	0.0499	PS
		888.6240	0.004	Galbeta-Cer
		888.6418	0.0218	LacCer
	889.62	889.5812	0.0388	PI

PCA, principal component analysis; PC, phosphatidylcholines; PE, phosphatidylethanolamines; PS, phosphatidylserines; PG, phosphatidylgylcerols; PA, phosphatidic acids; PI, phosphatidylinositols; TG, triglycerides; SM, sphingomyelins; GlcCer, glucosylceramide; GalCer, galactosylceramide; DG, diglycerides; Cer, ceramide; CerP, ceramide 1-phosphates; PnG, glycerophosphonocholines; LacCer, lactosylceramide; DA, discriminant analysis; ROI, regions of interest.

cellular and organismal functions. Lipids primarily have four different functions; (i) formation of membranes for the compartmentalization of cells and organelles, (ii) to act as an energy store and release energy when required for biological processes (iii) regulation of biochemical reactions by inducing the interaction activity between proteins and transient and permanent membranes and iv) signalling [12]. Biological cells, which undergo physiological change, such as migration and proliferation, initiate major morphological and cellular changes including membrane changes. Lipids acting as the lipid bilayer of cells and organelles are in direct contact with changes in intracellular and extracellular environments, which in turn result in chemical and structural changes in the lipids. The central dogma of molecular biology dictates that DNA makes RNA, which produce proteins (e.g. enzymes), which in turn make lipids, thus representing the phenome [12]. Therefore, lipids are becoming widely utilized as biomarkers for disease states, as changes in the lipidome provide insight into early biochemical anomalies or processes [13].

Immediately after a breach of skin integrity when the physical barrier becomes disrupted, the skin barrier repair/wound healing process becomes activated to repair the damaged area to prevent pathogens/ harmful materials entering the body as well as prevent fluid loss [14]. The formation of a new epithelial layer over the wound, to re-establish the barrier function, has been described as one of the most important events in wound healing. Therefore, re-epithelialization must occur quickly after damage to the skin to achieve the best healing outcome. Injury to the skin initiates a coordinated and ordered cascade of biological responses, which if not interrupted, progresses through all stages of the skin barrier repair/wound healing process [1]. Skin wound healing involves several overlapping stages, which include haemostasis, inflammation, proliferation and remodelling [4]. During the inflammation phase, which occurs immediately after injury, inflammatory cells (macrophages, neutrophils and monocytes) migrate to the wounded site via chemotactic signals [15]. Simultaneously, keratinocytes of the epidermis start to migrate, proliferate and differentiate to regenerate the epithelial layer across the damaged area [16]. Koivisto *et al.*, suggested basal keratinocytes may migrate as a sheet along the wound provisional matrix [16].

Figure 2 shows MS spectra acquired from the three different ROIs and differences in the signals associated with each region. The spectra collected from the dermis were very different from those collected from the wound site and epidermis. The epidermis and wound site spectra showed a greater number of analytes with greater signal intensity compared to the dermis. This may be due to the dermis consisting of fibroblasts, which are dispersed throughout the fibrin gel (which comprises the scaffold in this 3D cell model), compared to the keratinocytes of the epidermis, which are tightly connected to one another. Therefore, a greater number of lipids present in the same area provided a greater signal intensity. The spectra of the epidermis and wound site are also similar, because of the migration of keratinocytes into the wound site to close the damaged area. This is clearly observable in the H&E stained images of the sample (Fig. 2 inserts). These observations are in agreement with previous studies where keratinocyte migration and proliferation was initiated during the early stages of wound repair.

Mass spectrometry imaging visualizes the distribution of endogenous molecules, within tissue samples, by reconstructing false-coloured images based on the intensity of mass-to-charge (*m/z*) signals against pixel locations across the whole sample. There were differences in the signals found in ROIs, as shown in

Table II List of putative identification of ions from MS/MS profiling in negative ion mode in all three ROIs (dermis, wound site and epidermis) using LIPID MAPS structure database search (mass tolerance for product ions ±0.4 mDa)

Location	m/z	Theoretical m/z	m/z error	Putative identification	Empirical formula
Dermis	504.2478	N/A	N/A	No identification	N/A
	533.2899	N/A	N/A	No identification	N/A
	701.4029	701.5127	0.1098	PA [18 : 0/18 : 1 (11E)]	$C_{39}H_{74}O_8P$
	887.7372	887.5655	0.1717	PI [20 : 3 (8Z, 11Z, 14Z)/18 : 0]	$C_{47}H_{84}O_{13}P$
Epidermis	835.6749	N/A	N/A	No identification	N/A
	863.6806	N/A	N/A	No identification	N/A
	889.571	N/A	N/A	No identification	N/A
Epidermis/Wound site	742.6473	742.5839	0.0634	Glcβ-Cer	$C_{42}H_{80}NO_9$
Wound site	478.3276	N/A	N/A	No identification	N/A
	716.57	716.5236	0.0464	PE [16 : 0/18 : 1 (11E)]	$C_{39}H_{75}NO_8P$
	788.5557	788.5447	0.011	PS [18 : 0/18 : 1 (11E)]	$C_{42}H_{79}NO_{10}P$

ROI, regions of interest.

Table III List of identified metabolic pathways where metabolites changed in the wound site compared to the dermis based on the negative ion mode spectra.

Pathway associated with metabolite change	Number of metabolites changed in the pathway
Biosynthesis of unsaturated fatty acids	3
Ubiquinone biosynthesis	3
Purine metabolism	2
Arachidonic acid metabolism	1
Phenylalanine metabolism	1
Taurine metabolism	1
Propanoate metabolism	1
Glutathione metabolism	1
beta-Alanine metabolism	1

the MS images (Fig. 3A,B). Here specific m/z values could be used to visualize each area that is m/z 721.4 corresponded to the epidermis, m/z 725.4 correlated with the dermis and m/z 751.6 was shown to be specific to the wound site.

Principal component analysis-discriminant analysis of the spectra from each region of interest (Figs 4 and 5) was able to highlight a number specific m/z values associated with either the dermis, epidermis or wound site. Using the identified m/z values in combination with database search gave putative lipid identification for each m/z value (Table I). However, as many different lipids may have the same molecular formula therefore, possessing the same m/z value further analyses of species of interest was conducted.

MS/MS profiling was used to create lists of product ions for database search of the MS/MS spectra recorded from 11 m/z values of interest from Table I. From this data five putative lipids were identified as shown in Table II. Two glycerophospholipids (PA and PI) could be specifically associated with the dermis and two different glycerophospholipids (PE and PS) with the wound site/epidermis. Additionally, the wound site could be associated with a lipid which was part of the glycosylceramides class (Glcβ-Cer). Numerous studies have shown glucosylceramides are the glucosylated

intermediates for the synthesis of ceramides, which are essential for producing lamellar structures mediating the epidermal permeability barrier function and skin homoeostasis [17, 18]. Wounding the model disrupted the epidermis barrier function thus, stimulating keratinocytes to migrate and proliferate across the wound to close the damaged area. Therefore, the putative identification of glycosylceramides in the epidermis above the wound site may be associated with the keratinocytes repairing the wound and thus, involved in the skin barrier repair/wound healing process. These data suggest that glycosylceramides may be used as a biomarkers linked to early-stage wound healing.

The full scan MS data was also subjected to a metabolite search and analysis of accompanying metabolic pathways. Several metabolic pathways were identified as shown in Table III. The database found elevated signal intensities of 14 metabolites involved in nine different metabolic pathways in the wound site, compared to the dermis. These results indicate increased metabolite signal intensity correlated with increased metabolite production, which may be associated with wound healing. Three of the metabolites that had elevated signal intensities were part of the biosynthesis of unsaturated fatty acids pathway and studies have shown fatty acids including omega-3 fatty acids accelerate the re-epithelialization process [19]. Additionally, three metabolites were identified in the ubiquinone synthesis pathway. Studies of coenzyme Q10, which is a biosynthesized quinone known to possess anti-inflammatory effects have shown it to aid the skin barrier repair/wound healing process [20]. Furthermore, the purine metabolism pathway showed increased signal intensities of two metabolites and research has shown that non-adenine based purines promote cell proliferation and release growth factors, thus accelerating wound closure [21]. Other metabolites with raised signal intensities in the highlighted metabolic pathways in Table III have shown to improve the skin barrier repair/wound healing process by stimulating keratinocytes, inducing antioxidative responses or stimulating the biosynthesis of collagen [22–24]. Therefore, all these metabolites with elevated signal intensities in the wound site compared to the dermis are indicative of wound healing thus, supporting the lipid differences between the ROIs which may be used as biomarkers in the skin barrier repair/wound healing process.

Conclusion

The novel combination of the use of an *in vitro* LSE model with MSI allowed an in-depth molecular analysis of the skin barrier repair/wound healing process to be carried out. A number of lipids directly involved in the skin barrier repair/wound healing process were identified, indicating these as potential biomarkers for further study and eventual use within the clinic. Validation of the identified species as time-dependent biomarkers would assist in the determination of which stage of the skin barrier repair/wound healing process the wound is in. This would facilitate the provision of best treatment to patients with wounds.

References

1. Beldon, P. Basic science of wound healing. *Surg.* **28**, 409–412 (2010).
2. Gosain, A. and DiPietro, L.A. Aging and wound healing. *World J. Surg.* **28**, 321–326 (2004).
3. Korting, H., Schöllmann, C. and White, R. Management of minor acute cutaneous wounds: importance of wound healing in a moist environment. *J. Eur. Acad. Dermatol. Venereol.* **25**, 130–137 (2011).
4. Guo, S. and DiPietro, L. Factors affecting wound healing. *J. Dent. Res.* **89**, 219–229 (2010).
5. Sen, C.K., Gordillo, G.M., Roy, S., *et al.* Human skin wounds: a major snoballing threat to public health and economy. *Wound Repair Regen.* **2009**, 763–771 (2009).
6. Morgan, T. Are your wound management choices costing you money? *J. Community Nurs.* **29**, 17–20 (2015).
7. Thomsen, K., Trøstrup, H., Christophersen, L., Lundquist, R., Høiby, N. and Moser, C. The phagocytic fitness of leucopatches may impact the healing of chronic wounds. *Clin. Exp. Immunol.* **184**, 368–377 (2016).
8. Guest, J.F., Ayoub, N., McIlwraith, T., *et al.* Health economic burden that wounds impose on the National Health Service in the UK. *BMJ Open* **5**, e009283 (2015).
9. Schwamborn, K. and Caprioli, R.M. Molecular imaging by mass spectrometry–looking beyond classical histology. *Nat. Rev. Cancer* **10**, 639–646 (2010).
10. Yang, K. and Han, X. Lipidomics: techniques, applications, and outcomes related to biomedical sciences. *Trends Biochem. Sci.* **41**, 954–969 (2016).
11. Cajka, T. and Fiehn, O. Comprehensive analysis of lipids in biological systems by liquid chromatography-mass spectrometry. *Trends Analyt. Chem.* **61**, 192–206 (2014).
12. Stephenson, D.J., Hoeferlin, L.A. and Chalfant, C.E. Lipidomics in translational research and the clinical significance of lipid-based biomarkers. *Transl. Res.* **189**, 13–29 (2017).
13. Fernandis, A.Z. and Wenk, M.R. Lipid-based biomarkers for cancer. *J. Chromatogr. B Analyt. Technol. Biomed. Life Sci.* **877**, 2830–2835 (2009).
14. Evans, N.D., Oreffo, R.O., Healy, E., Thurner, P.J. and Man, Y.H. Epithelial mechanobiology, skin wound healing, and the stem cell niche. *J. Mech. Behav. Biomed. Mater.* **28**, 397–409 (2013).
15. Koh, T.J. and DiPietro, L.A. Inflammation and wound healing: the role of the macrophage. *Expert Rev. Mol. Med.* **13**, e23 (2011).
16. Larjava, H., Häkkinen, L. and Koivisto, L. Re-epithelialization of wounds. *Endod. Topics* **24**, 59–93 (2012).
17. Tsuji, K., Mitsutake, S., Ishikawa, J., *et al.* Dietary glucosylceramide improves skin barrier function in hairless mice. *J. Dermatol. Sci.* **44**, 101–107 (2006).
18. Amen, N., Mathow, D., Rabionet, M., *et al.* Differentiation of epidermal keratinocytes is dependent on glucosylceramide: ceramide processing. *Hum. Mol. Genet.* **22**, 4164–4179 (2013).
19. McDaniel, J.C., Massey, K. and Nicolaou, A. Fish oil supplementation alters levels of lipid mediators of inflammation in microenvironment of acute human wounds. *Wound Repair Regen.* **19**, 189–200 (2011).
20. Choi, B.S., Song, H.S., Kim, H.R., *et al.* Effect of coenzyme Q10 on cutaneous healing in skin-incised mice. *Arch. Pharm. Res.* **32**, 907–913 (2009).
21. Jiang, S., Zavitz, C.C.J., Wang, J., *et al.* Non-adenine based purines accelerate wound healing. *Purinergic Signal.* **2**, 651–661 (2006).
22. Yin, J., Bai, S., Wu, F., Lu, G. and Yang, H. Effect of nitric oxide on the activity of phenylalanine ammonia-lyase and antioxidative response in sweetpotato root in relation to wound-healing. *Postharvest Biol. Technol.* **74**, 125–131 (2012).
23. Sasso, O., Pontis, S., Armirotti, A., *et al.* Endogenous N-acyl taurines regulate skin wound healing. *Proc. Natl Acad. Sci. U.S.A.* **113**, E4397–E4406 (2016).
24. Nagai, K., Suda, T., Kawasaki, K. and Mathuura, S. Action of carnosine and beta-alanine on wound healing. *Surgery* **100**, 815–821 (1986).